Remote Sensing of Environment 186 (2016) 637–651

Contents lists available at ScienceDirect

Remote Sensing of Environment

journal homepage: www.elsevier.com/locate/rse

Thermal infrared remote sensing of urban heat: Hotspots, vegetation, and an assessment of techniques for use in urban planning

Andrew M. Coutts [a,b,*], Richard J. Harris [a], Thu Phan [a], Stephen J. Livesley [c], Nicholas S.G. Williams [c], Nigel J. Tapper [a,b]

[a] School of Earth, Atmosphere and Environment, Monash University, Australia
[b] CRC for Water Sensitive Cities, Australia
[c] School of Ecosystem and Forest Sciences, University of Melbourne, Australia

ARTICLE INFO

Article history:
Received 17 August 2015
Received in revised form 12 August 2016
Accepted 12 September 2016
Available online 3 October 2016

Keywords:
Urban climate
Planning tools
Thermal infrared remote sensing
Urban greening
Heat mitigation

ABSTRACT

In order to mitigate areas of high urban air temperature (or 'hotspots'), advice and tools are currently being sought to help inform urban planning and decision making around urban greening. One potential tool receiving growing interest is the use of thermal imagery for identifying hotspots, however this relies on the assumption that patterns in land surface temperature (LST) coincide with patterns in air temperature. This study explores the capacity of very high resolution (VHR), airborne thermal infrared (TIR) remotely sensed data to identify hotspots at a neighbourhood and street scale resolution. As such it assesses whether VHR TIR remote sensing is an appropriate tool for urban planning and urban greening decision making. In partnership with a local municipality in Melbourne, Australia, VHR (0.5 m) daytime and night time TIR images were captured during warm summertime conditions in February 2012. We found that VHR TIR data certainly identified locations of high LST that could be prioritized for urban greening, however at very high resolutions, VHR TIR data could not identify hotspots because patterns in LST did not strongly correlate with patterns of high air temperature. When VHR TIR data was aggregated to a coarser resolution, it could be used at the neighbourhood-scale to identify hotspots due to greater confidence that areas of high LST do represent air temperature hotspots. Increased vegetation proportion was associated with a reduction in LST for both the day and night meaning urban greening can be used to mitigate hotspots and should be prioritized in wide, open streets where building shade is less. While VHR TIR remote sensing may be an attractive option, this study shows it is not a suitable tool to help inform urban planning and urban greening decision making as the capture, post-processing and interpretation requirements and costs of delivering a high quality product are prohibitive for many end users. We suggest that those seeking to use thermal imagery to identify hotspots in the urban landscape, strongly consider more accessible and cheaper satellite remote sensing products (such as Landsat). VHR TIR derived LST may be useful in designing urban spaces for improved human thermal comfort and focusing on a small region of interest, but the numerous complexities and limitations of the data must be recognized.

1. Introduction

Increasing urban vegetation is widely recognized as a key approach to mitigating urban heat through evapotranspiration and shading (Dimoudi and Nikolopoulou, 2003; Chen and Wong, 2009). Several studies have modelled a reduction in air temperature from an increase in urban vegetation cover (Zhou and Shepherd, 2010; Loughner et al., 2012; Rosenzweig et al., 2009), while satellite remote sensing studies have demonstrated that greater vegetation cover corresponds with reduced land surface temperature (LST) (Li et al., 2012; Rogan et al., 2013; Klok et al., 2012). Ensuring that urban areas have sufficient vegetation cover and regular distribution of vegetated open space is important to reduce daytime heat storage in the urban environment (Honjo and Takakura, 1990). Further, maintaining adequate soil moisture via irrigation and water sensitive urban design is desirable to support healthy vegetation and promote evapotranspiration (Goldbach and Kuttler, 2012; Coutts et al., 2013). Urban planners and designers are recognizing the growing need to create more attractive, thermally comfortable and sustainable cities, especially as urban populations expand and climatic variability and extremes increase.

In response to elevated urban temperatures and the knowledge of relations between high urban air temperature and adverse heat-related health outcomes (e.g. mortality and heat related illness) (Loughnan et al., 2013), local municipalities are exploring how to best implement urban greening to improve urban climates. Unfortunately, there is little practical guidance available, and as Bowler et al. (2010) concluded from

* Corresponding author at: School of Earth, Atmosphere and Environment, Monash University, Room 205, Building 28, Wellington Rd, Clayton, Victoria, 3800, Australia.
E-mail address: Andrew.Coutts@monash.edu (A.M. Coutts).

http://dx.doi.org/10.1016/j.rse.2016.09.007
0034-4257/

a review of urban greening for cooling in cities: *"The current evidence base does not allow specific recommendations to be made on how best to incorporate greening into an urban area"* (pg 147), though recent research has begun to address this void (Norton et al., 2015). The lack of guidance presents a problem because limited funds are available to city or municipal governments to establish and maintain public green space and street trees over the long term, so prioritizing investment to achieve heat mitigation objectives is paramount. Urban planners and designers need readily accessible, cheap and rapidly available tools to support decision making processes.

In a bid to inform heat mitigation strategies and the prioritized implementation of urban vegetation cover, some local municipalities are investigating the use of thermal imagery as a tool to identify 'hotspots'. Hotspots are defined here as areas of relatively higher air temperature (T_a). Using thermal imagery to identify hotspots relies on the assumption that areas of high T_a coincide with areas of high LST (i.e. higher LST leads to higher T_a, which leads to higher risk of heat stress). Aniello et al. (1995) used Landsat Thematic Mapper (TM) satellite data (120 m) to map LST in Dallas, Texas, noting that areas of high LST occurred most frequently where tree cover was lacking, such as business districts and shopping complexes. In contrast, a number of local municipalities in Australia have experimented with very high resolution (VHR) (e.g. <5 m), airborne thermal infrared (TIR) remote sensing to inform greening strategies and tree placement as it provides a very detailed spatial picture of the LST of the urban surface. Previous studies using VHR TIR data have identified important landscape features that influence LST including the amount of sealed (impervious) surfaces (Kottmeier et al., 2007), the irrigation of green space and amount of tree cover (Spronken-Smith and Oke, 1998), and street geometry (Bärring et al., 1985). VHR TIR remote sensing can potentially provide detailed information for targeted urban greening at the household and street-scale and is an excellent communication tool for local planning authorities and residents.

Despite the attractiveness of VHR TIR remote sensing, the collection, analysis and interpretation of the data are not straight forward, and there are several limitations. Again, TIR remote sensing provides a spatial picture of LST rather than T_a and a key assumption is that patterns in LST can be used as a surrogate for patterns in T_a. Saaroni et al. (2000) observed similar patterns in surface and air temperatures using high resolution (2 m) airborne TIR remote sensing in Tel Aviv, Israel. Similarly, Nichol et al. (2009) measured a close relationship between the surface and air temperature in Hong Kong (ASTER satellite data, 90 m resolution). However, others state there is no simple, general relation between measured air temperature and remotely sensed LST data (Voogt and Oke, 2003; Tomlinson et al., 2011).

Several other issues should be considered in the collection and application of VHR TIR remote sensing data for urban planning. Industry providers of VHR TIR data may or may not have tested, calibrated, or evaluated their TIR camera for an urban landscape scenario. What is often provided is an image of surface brightness temperature that has not been corrected for atmospheric effects or emissivity. Correction for emissivity needs to occur but is difficult at such high resolutions because individual surface types are identifiable and are highly varied. Correcting VHR TIR remote sensing data using a uniform emissivity value (e.g. Pu et al., 2006) is not appropriate, while Temperature – Emissivity Separation algorithms (e.g. Gillespie et al., 1998) require multiple bands in the thermal spectral range in order to be applied. Also, TIR data depends on the viewing angle of the sensor and airborne based plan (bird's eye) views of the surface often neglect the LST of walls and obstructed surfaces such as below tree canopies (Voogt and Oke, 2003), all of which contribute to the microclimate of the urban canopy layer (the layer of air below the mean height of buildings and vegetation). The complex nature of the urban surface due to large buildings and other urban structures results in highly variable patterns of LST. This leads to directional variations in outgoing longwave radiation from these surfaces (thermal anisotropy) (Voogt and Oke, 1998) which influences observed radiances and is also often ignored. Furthermore, the low temporal frequency of VHR TIR data capture should also be considered, as LST patterns will vary greatly over time with changes in thermal admittance, surface moisture, net radiation, and differences in near-surface atmospheric conditions (Voogt and Oke, 2003). Without a consideration of these various issues, there is a risk of misinterpretation of TIR data (Roth et al., 1989).

In collaboration with a local municipality, this study explores the potential application of VHR TIR remote sensing to identify hotspots and inform urban land use planning and strategies for heat mitigation using urban greening. The aim of urban greening is to intentionally modify surface radiative and energetic processes by replacing impervious urban surfaces of high thermal admittance with trees, green walls and green roofs (that are well supplied with water) that have lower thermal admittance than urban surfaces and allow infiltration into the soil. As a result, heat conduction is reduced and evapotranspiration is promoted leading to reduced LST. The combination of reduced LST and greater evapotranspiration means there is less sensible heating of the atmosphere, thereby improving the thermal environment for urban populations. Trees are particularly effective as they provide shade to urban surfaces and can access deep water reserves (Coutts et al., 2013). Using VHR TIR remote sensing captured during a heatwave, we explore relationships between LST and vegetation cover, and associations between LST and near surface T_a. Drawing primarily on VHR airborne TIR remote sensing, and supported by satellite TIR remote sensing, this study seeks to investigate the following questions:

1) Can VHR TIR remote sensing be effectively used to identify hotspots (areas of relatively high T_a) at the neighbourhood-scale and the street-scale and where to prioritise urban greening?
2) How does vegetation cover influence VHR TIR derived LST and the potential development of hotspots?
3) Is VHR TIR remote sensing a suitable tool to provide appropriate information to inform urban greening interventions for urban heat mitigation?

In tackling these questions, we seek to provide guidance on how useful TIR remote sensing can be for urban planning, the most effective approaches for collecting and applying TIR remote sensing data, and an understanding of what can be achieved given the limitations. This guidance is provided with a focus on the end user, such as local municipal staff, and their capacity to appropriately acquire, interpret and apply remotely sensed TIR data for use in urban land use and heat mitigation planning.

2. Methodology

2.1. Acquisition of high resolution TIR remote sensing data

The City of Port Phillip (CoPP), a local municipality in Melbourne Australia, commissioned VHR, airborne TIR remote sensing in the summer of 2011–12. The objective was to use this high resolution TIR data to inform the implementation of a policy of increased tree canopy cover, by identifying the hotspots within their municipality using thermal imagery and then prioritise these for cooling through urban greening (CoPP, 2010). A collaborative project was established between CoPP, adjacent local municipalities, the Victorian state government, consultants and university researchers in a bid to explore and draw as much value from the thermal imagery as possible. This collaborative project sought to establish a guide for local and state governments on the use and applicability of high resolution TIR for heat mitigation and adaptation planning in urban landscapes. For this purpose, hotspots are defined as areas of relatively high T_a, meaning any urban greening implementation based on thermal imagery relies on the assumption that areas of high LST coincide with areas of high air temperature. This assumption will be tested here.

Following a review of previous studies (e.g. Saaroni et al., 2000; Quattrochi and Ridd, 1994; Kottmeier et al., 2007) we developed a protocol for the collection of VHR airborne TIR data outlined in Table 1. The flight protocol required TIR data capture at both solar noon and pre-dawn on the following day, during warm, clear sky conditions with low wind speeds to observe the largest possible differences in LST. Setting rigid thresholds for particular flight conditions (e.g. a threshold temperature) risks missing suitable opportunities to capture data, and a degree of flexibility is needed. Flight duration should also be brief (< 60 min) to avoid large changes in LST during the course of the flight. Advantages of airborne TIR remote sensing over satellite TIR remote sensing include the ability to control the capture time according to suitable climatic conditions, and the ability to vary resolution according to height of flight.

On 25 February 2012 (late summer), a daytime and a night time flight was undertaken by service providers engaged by the CoPP. For the data capture, the flight protocol was largely followed by CoPP, their consultants and the service provider, but the resolution was higher (extending the flight duration), and the night time TIR data capture occurred at midnight (Australian Eastern Daylight Time AEDT). No corrections were made to LST to account for surface warming/cooling that inevitably occurred during the course of the flight. The altitude flown was 2400 ft (731 m) which produced an image resolution of 0.5 m. The camera used was a FLIR A615 with a spectral range of 7.5–13 μm and a thermal sensitivity of <0.05 °C at 30 °C and an accuracy of ± 2 °C or 2% of the reading. The camera's field of view was 25° × 18.8°. The flight coincided intentionally with a period of high summer temperature, in which the maximum daytime air temperature reached 37.1 °C. The mean 30 year (1981–2010) maximum daily air temperature for February in Melbourne was 25.8 °C, so this period was well above average, although fell short of some of the more extreme heat days that can be experienced in Melbourne (e.g. up to 46 °C). The meteorological conditions at the time were typical of summertime heatwaves and generally support canopy layer urban heat island (UHI) development in Melbourne (Morris and Simmonds, 2000) with a high pressure system situated off the south-east coast of Australia supporting clear sky conditions, and bringing warm, dry continental air from central Australia to the state of Victoria.

The VHR TIR data was provided to the university researchers for post-processing and analysis. While ideal conditions were achieved for the data acquisition, a primary limitation was that only one day and night time dataset were obtained. As highlighted above, the temporal variations in LST can be very large, especially at high resolutions, as a result of shading patterns, changes in surface moisture and thermal admittance, and meteorological conditions. Several studies have explored the systematic and random temporal variations of remotely sensed thermal data including MODIS (Duan et al., 2014), however capturing multiple high resolution airborne TIR data is prohibitive. Another limitation was that effective thermal anisotropic effects were ignored. Vertical surfaces (walls) 'seen' by the sensor can have sharply contrasting surface temperature patterns depending on urban geometry, sun position and sensor field of view (Voogt and Oke, 1998). These directional variations are of similar magnitude to atmospheric corrections (Voogt and Oke, 1998).

2.2. Land surface classification

To assist in the post-processing of the TIR data and its interpretation, a detailed land surface classification was completed. This provided necessary information to explore the influence of land surface characteristics on LST and identify the land surface characteristics that support the development of hotspots. Several auxiliary data sources were available from the CoPP to assist in classifying the surface. This included aerial imagery (0.5 m aerial photo from 13 March 2012 in 4 bands: blue, green, red and near-infrared), hyperspectral data (0.5 m resolution, captured in November 2011, 80 bands with wavelength from 0.410 μm to 0.983 μm) and LiDAR data (2007 with ground and first return provided). LiDAR data were used to construct a Digital Surface Model (DSM) and Digital Elevation Model (DEM) in ArcGIS 10.2 (ESRI, 2013). The normalized Digital Surface Model (nDSM) was determined by subtracting the DEM from the DSM. The nDSM was used to differentiate high elevated objects (such as trees or buildings) from the ground surface (such as roads or very low shrubs).

Based on the spectral signatures of the aerial imagery, hyperspectral data, and the raw TIR data, as well as the LiDAR data, a rule-based image processing approach was designed in Definiens eCognition Developer 8.7 (Definiens, 2013) to classify land cover into the six different land surface types: 1. vegetation (including tree, grass and other vegetation), 2. asphalt, 3. concrete, 4. water, 5. buildings and 6. other (including bare ground/shadow) (Fig. 1a). This land surface classification was used to determine vegetation cover and to independently assign an emissivity value to each surface type. Surface changes over the period of data collection of these sources were assumed to be negligible. The overall accuracy of the land surface classification (confusion matrix) was 87.8% with a kappa coefficient of 0.843 indicating a good agreement between classification and sampled land cover classes. The classification was very good at distinguishing building rooftops from ground level surfaces (important for emissivity corrections) and distinguishing vegetation (for understanding relations with LST), while most of the errors stemmed from areas of shadow where surfaces were difficult to classify.

2.3. Ground evaluation of LST

We sought to evaluate or 'ground-truth' the LST provided by the airborne TIR data to provide some assessment of the quality of the product in predicting the temperature of different surface types. Five sites were established within the CoPP in January 2012 in anticipation of the summer flight. These five sites were established over a range of surface

Table 1
Flight protocol for the collection of high resolution airborne thermal remote sensing data on 25–26 February 2012 (AEDT is Australian Eastern Daylight Time; T_{max} is maximum daily air temperature).

	Protocol	25–26 February 2012
Flight time	Day: Solar maximum, between 13:00 and 15:00	Day: 13:00 to 15:00 AEDT
	Night: Pre-dawn, ideally between 03:00 and 05:00	Night: 00:00 to 02:00 AEDT
Resolution	1 to 5 m	0.5 m
Flight duration	<60 min	120 min
Ground evaluation	Fixed ground monitoring sites using IR temperature sensors	Day: five sites
		Night: seven sites
Meteorological requirements	Preferably 2 to 3 consecutive days of warm sunny conditions	23 Feb. 2012: T_{max} = 25.8 °C
		24 Feb. 2012: T_{max} = 37.1 °C
		25 Feb. 2012: T_{max} = 37.1 °C
	Clear skies and low wind speeds are critical	0–1 octas
		Day: 2 m s^{-1}; Night: 0.3 m s^{-1}

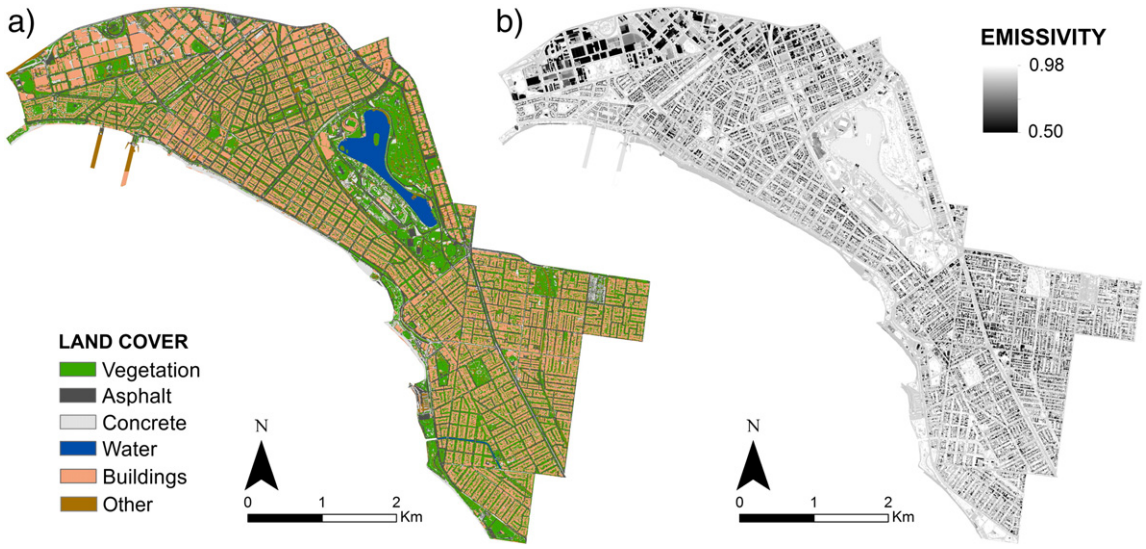

Fig. 1. a) Land cover type and b) emissivity throughout the City of Port Phillip.

types, in secure locations, that provided a large area of flat, homogeneous surface cover for simple matching with the high resolution TIR data, and included: grass, gravel, concrete, bare ground (clay) and metal roof. Two temporary sites were also installed for the period of the night time flight (grass and asphalt). These seven sites consisted of an infrared radiometer (SI-121, Apogee Instruments), and a temperature and relative humidity sensor (HMP45C, Campbell Scientific) installed at a height of 1.5–2 m above each surface. Data were collected by dataloggers (CR1000, Campbell Scientific), sampled every 30 s and averaged to 5 min. No atmospheric correction was applied to the ground based sensors.

2.4. Atmospheric and emissivity corrections

The TIR data captured were surface brightness temperature (or spectral radiance L) and therefore needed to be corrected for atmospheric and emissivity effects to determine a surface blackbody radiance over the waveband of response. The spectral radiance (L) observed at a sensor at altitude (h) and view angle (θ) to the normal, is a combination of the surface radiance (L_0), reflected radiance (L_{sky}), and the atmospheric-path longwave emission from the atmosphere between the ground and the sensor (L_a). The surface radiance L_0 can then be used to calculate the true LST. Following Voogt (2000), the spectral radiance is given by:

$$L(h,\theta) = \tau(h,\theta)\varepsilon L_0 + \tau(h,\theta)(1-\varepsilon)L_{sky} + L_a \quad (1)$$

where ε is the emissivity and τ is the atmospheric transmissivity. An atmospheric correction was applied to the data incorporating the spectral response function of the sensor using MODO5 (ReSe Applications Schläpfer) which incorporates the model MODTRAN-5 (Berk et al., 1989; Berk et al., 2000) providing estimates of τ and L_a. Atmospheric soundings were not collected at the time of the flights, so the mid-latitude summer standard atmosphere of MODTRAN-5 was used, along with the standard urban aerosol profile and scaled for H_2O in the atmospheric column for Melbourne (Mieruch et al., 2008; Noël et al., 2004). This representation of the incoming radiation approximates the urban canopy to be a flat surface. Average L_{sky} observed for the duration of the flights was taken from nearby Monash University (CGR3, Kipp and Zonen).

To assign a temperature value to a surface, an emissivity value must be assigned (Artis and Carnahan, 1982). Emissivity correction of VHR TIR data varies between studies. Voogt (2000) applied a bulk emissivity correction using an assumed emissivity value of 0.95, but for low emissivity surfaces (primarily metal roofs), values were reassigned to the mean LST of building rooftops. Kottmeier et al. (2007) applied literature based emissivity corrections, but noted that resulting LST may be underestimated by up to 2 °C from the actual LST. Lo et al. (1997) used radiance energy values instead of temperatures to avoid the need for emissivity corrections. In this study, each land surface classification type (Fig. 1a) was assigned an emissivity value (Fig. 1b) which was applied in the calculation of surface radiance. Standard emissivity values were applied based on literature values for each surface type (Table 2), and also for the established ground evaluation points. For buildings however, the rooftop materials were very diverse, from concrete tiles to various types of metal roofs, making a single value for the emissivity of all rooftops inappropriate (see Section 2.5). The emissivity of the steel rooftop evaluation site was determined as 0.5 (see Section 2.5). Surfaces classified as 'other' were assigned an average of the ground surfaces of 0.96. The VHR TIR data showed encouraging results for LST when compared to the ground evaluation sites (Table 3), with very similar LST calculated for both the daytime and night time. Some small discrepancies remain, and could stem from slightly incorrect estimates of emissivity and sensor view angles. This result gives confidence in the quality of the VHR TIR data. Only the clay site (a red porous tennis court) showed substantial differences during the day and was likely a result of court watering.

2.5. Establishing an emissivity correction for building rooftops

Determining a single emissivity value for building rooftops proved especially difficult as values varied dramatically in the literature,

Table 2
Emissivity values used in the calculation of land surface temperature of the high resolution thermal infrared remote sensing data and their source.

Surface type	Emissivity	Source
Concrete	0.94	Oke, 1987
Water	0.97	Oke, 1987
Grass	0.98	Geiger et al., 2009
Trees	0.98	Oke, 1987
Asphalt	0.95	Oke, 1987
Building rooftops	0.5–0.94	See Section 2.5 and Appendix A
Clay	0.95	Arya, 2001
Gravel	0.92	Harman, 1994

Table 3
Comparison of corrected surface temperatures from the ground based monitoring stations (Ground) and the land surface temperature (°C) from the thermal image (TIR) and the standard deviation (for a circle of radius 3 m aligned with the ground based sensor field of view) at the time of the day and night time flights. Times are Australian Eastern Daylight Time (AEDT).

Surface	Day time (25 Feb. 2012)			Night time (26 Feb. 2012)		
	Time	Ground	TIR	Time	Ground	TIR
Gravel	13:20:46	57.1	57.3 ± 0.6	1:31:49	29.3	32.3 ± 0.3
Clay	13:48:31	59.6	49.4 ± 5.0	1:48:20	23.7	23.5 ± 0.8
Grass (a)	13:38:02	62.4	62.1 ± 2.2	1:44:13	16.4	19.6 ± 0.9
Metal roof	13:32:04	50.0	51.0 ± 1.4	1:39:03	10.0	12.2 ± 10.1
Concrete	12:45:45	52.7	53.5 ± 0.4	0:53:41	33.6	34.1 ± 0.4
Asphalt	–	–	–	1:49:11	18.1	21.8 ± 0.2
Grass (b)	–	–	–	1:49:11	29.3	29.1 ± 0.2

especially for metal roofs, and values vary with roof material (e.g. galvanized steel, zinc plated aluminium) and condition (e.g. amount of rust, dirt). Considering the TIR radiance data for the CoPP, some bright metal roofs displayed extremely low radiance values (e.g. between 320 W m^{-2} and 420 W m^{-2} for the daytime and 280 W m^{-2} to 380 W m^{-2} at night) compared with tiled, concrete and other metal roofs (e.g. ranging between 430 W m^{-2} and 830 W m^{-2} for the daytime and 380 W m^{-2} and 500 W m^{-2} at night). Further, distinguishing tiled and concrete roofs from metal roofs in the land surface classification was difficult without a high quality hyperspectral image captured at the same time as the TIR data, so only one rooftop class was determined. As such, a single emissivity value for roofs was recognized as being insufficient as it would lead to large errors for this surface type. Consequently, we developed a linearly varying emissivity (between 0.5 and 0.94) for roofs based on the range of radiance values observed across the night time TIR data (see Appendix A) which resulting in a good agreement between the VHR TIR data and the ground evaluation data.

2.6. Air temperature observations

A key assumption when using TIR remote sensing for the identification of hotspots is that LST can be used as a proxy for air temperature (T_a). Correlations between the two tend to be stronger under more stable atmospheric conditions, becoming decoupled under higher wind velocities (Stoll and Brazel, 1992), and so correlations improve at night when low level advection is reduced (Unger et al., 2010). Similar to previous work (Saaroni et al., 2000; Hart and Sailor, 2009; Voogt and Oke, 2003) we undertook two automobile transects at the same time as the night time flight to explore relations between LST and T_a. The two separate T_a transects were collected at different spatial scales: 1) a long, west to south-east transect across Melbourne for comparison with satellite derived LST (see MODIS description in Section 2.7) and the canopy layer UHI, and 2) a short transect within the CoPP for comparison with the VHR TIR data (Fig. 2). Air temperature was measured using a temperature and relative humidity sensor (HMP45C, Campbell Scientific) within a Gill 10-plate radiation shield, and position was tracked using a Global Positioning System (GPS16X-HVS GPS Receiver, Garmin) mounted above the passenger side window. Data were recorded every 10 s (CR1000, Campbell Scientific). The travel times were 117 min and 80 min for the west to south-east and CoPP transects respectively and the average speed of the vehicles were 28.1 km h^{-1} and 18.1 km.h^{-1} respectively. The movement of the vehicles aspirated the sensors and data were excluded when the vehicles were stationary. The T_a data were corrected for background temperature changes over the period of each transect to 1:00 AEDT using temperature changes recorded at the rooftop ground evaluation site. The cross-city transect showed a canopy layer UHI was present at 1:00 AEDT, and the central city area was several degrees warmer than surrounding rural areas with a maximum UHI intensity of 8.1 °C, although T_a along the transect was highly variable. The transect passed by the north-east corner of the CoPP boundary (Fig. 2) where T_a was up 6.2 °C warmer than the coolest rural areas and highlights that the CoPP is one region where urban warming is a

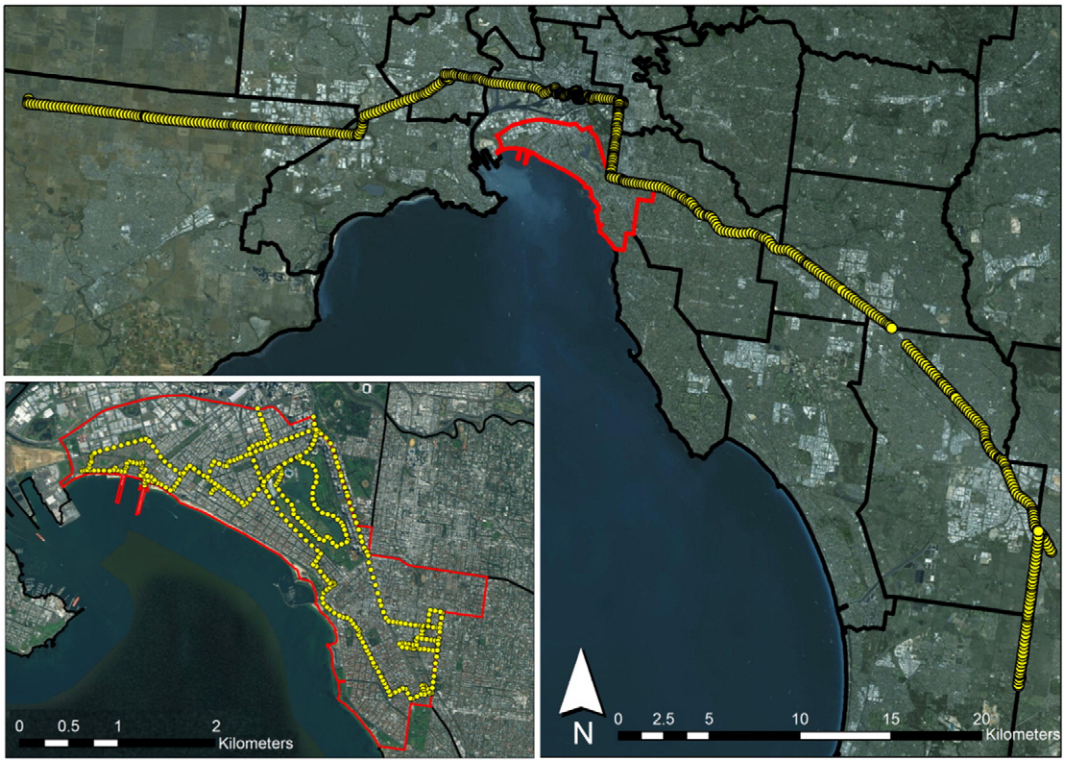

Fig. 2. Automobile transects conducted at the time of the night time airborne thermal remote sensing flights on the morning of 26 February 2012. The red boundary is the City of Port Phillip.

concern and justifies the closer research focus and consideration of greening for urban heat mitigation.

2.7. Acquisition of satellite TIR remote sensing data

Coarse resolution, satellite TIR remote sensing data were obtained for the same day as the VHR airborne TIR data. The satellite TIR data provided further opportunity to explore relationships between LST and T_a, and provided the ability to compare different remote sensing approaches. A Landsat 7 ETM+ image from the same day as the thermal flights (25 February 2012, at approximately 11:00 AEDT) was sourced. This also provided an opportunity to explore the practicalities of collecting and using the two remotely sensed data products in the urban planning context. Both the raw Landsat and Landsat surface reflectance dataset captured on 25 February 2012 were obtained (USGS, 2014). The resolution of the Landsat 7 ETM+ thermal band 6 is 60 m, which is resampled to 30 m. The Landsat surface reflectance dataset was radiometrically corrected and both cloud and cloud shadow detection conducted using the Second Simulation of a Satellite Signal in the Solar Spectrum (6S) radiative transfer models in specialized software named Landsat Ecosystem Disturbance Adaptive Processing System (LEDAPS) (USGS, 2014). To allow for a comparison between datasets, the VHR TIR radiance data was aggregated to 60 m and then resampled to 30 m using cubic convolution (the same resampling method used for Landsat 7 ETM+ data). The brightness temperature was used in the comparison so as to avoid any discrepancies that might arise from emissivity corrections for each dataset.

City-scale, daytime and night time MODIS satellite TIR data were also obtained and processed for the February 2012 dates (Fig. 3). The MODIS/Aqua Land Surface Temperature and Emissivity (LST/E) product (MYD11A1) is daily, tiled-based and gridded in the sinusoidal projection at 1 km spatial resolution (LP DACC, 2014). This product was chosen because the overpass time was closest to CoPP high resolution thermal image acquisition time. Version 005 (V5) was chosen for searching and acquiring data. The image output was also set as the same projection coordinate system as other GIS datasets in the project (GDA1994, zone 55). The V5 MYD11A1 are validated to Stage-2 through field campaigns and radiance-based validation studies (LP DACC, 2014). The zenith viewing angle for each of the MODIS images for the CoPP was 34 degrees (daytime) on 25 February 2012 and 27 degrees (night time) on 26 February 2012. The NDVI (MODIS 250 m) was also obtained (Rouse et al., 1974; Tucker, 1979) allowing an assessment of vegetation cover across metropolitan Melbourne and for examining the relationship between LST, T_a and vegetation cover at the city-scale.

The MODIS satellite remote sensing provided important context for the examination of the high resolution TIR data. During the day, the CoPP displayed a similar LST to the wider metropolitan Melbourne area (Fig. 3) with higher LST than the outskirts of the city. At night, the CoPP was amongst the warmest municipalities in terms of LST, suggesting that the CoPP is a high priority area for urban heat mitigation. The influence of the urban landscape, in terms of both extent and density, was clearly distinguishable across Melbourne at night, where the boundary of urban development was well defined by a surface UHI.

2.8. Identifying hotspots

The objective of this work was to use the VHR TIR data to identify hotspots assuming that areas of high LST coincide with areas of high T_a, however an appropriate scale must first be defined. If the scale of interest is to identify neighbourhoods with higher T_a than those within the broader urban landscape (in this case, the CoPP), the data needs to be aggregated to a coarser spatial resolution. The choice of spatial resolution will influence the location and intensity of hotspots and aggregation results in thermal surfaces becoming more spatially homogeneous as pixel distinctions are smoothed (Weng et al., 2004) and raises the issue of the modified areal unit problem. We chose to aggregate the data to align with the smallest of the Australian Bureau of Statistics (ABS) statistical areas (Statistical Area Level 1, or SA1) which also allows for comparisons with other accessible ABS data such as average age or socio-economic status if desired (Norton et al., 2015). Here, we calculated the average LST for each SA1 (227 in total with an average area of 0.09 km^2) in the CoPP and then categorized them into three classes of priority for urban greening: Low, Medium and High (using quantile classification). The aggregation of the data allowed for the rapid identification of neighbourhood-scale hotspots and a clear and simple approach for identifying *where* best to target areas for urban heat mitigation strategies.

If the scale of interest is to identify streetscapes, public spaces or other landscape features with high T_a within a particular area, then VHR TIR remote sensing can provide high resolution LST data. We chose an area of interest (AOI) with multiple land cover types and building morphologies to explore in greater detail. The area, known as 'South Melbourne Central', is a designated activity centre where future growth is expected and urban development is guided by a 'Structure Plan and Implementation Strategy', and an 'Urban Design Framework' (CoPP, 2007). It was also selected based on the decision framework for urban heat mitigation developed by Norton et al. (2015) which recommends targeting areas for urban greening that display high LST, high population vulnerability, and high population activity (e.g. where people move and congregate). We chose to define individual urban canyons throughout the AOI into street segments, and neglect rooftops. For each segment, the mean canyon LST was calculated and categorized into three classes of priority for urban greening: Low, Medium and High (using quantile classification) to identify *where* best to target areas for urban heat mitigation strategies.

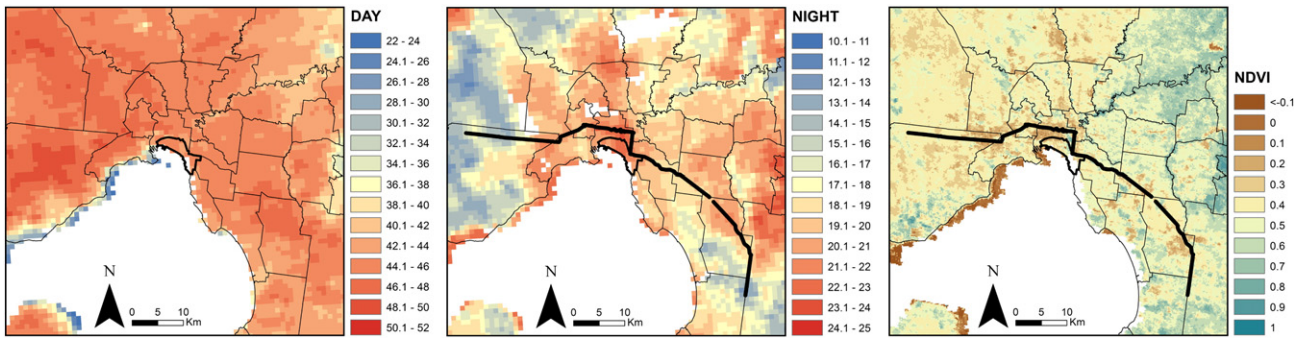

Fig. 3. Land surface temperature derived from MODIS (1 km) at 13:00 EDT 25 February 2014 (DAY) and 1:00 EDT 26 February 2014 (NIGHT); and MODIS derived NDVI (250 m). The Melbourne municipalities are displayed, and the night time west to south-east automobile transect is presented in the night time and NDVI images. White areas are missing data due to clouds and water surfaces.

2.9. Vegetation and LST relations

Using the land surface classification that derived the true vegetation cover across the CoPP, we sought to explore the relationship between vegetation cover and LST. The VHR TIR data were aggregated to a mean LST at a resolution of 30 m for the entire CoPP and compared with percentage vegetation cover, binned into 10% categories. For the AOI, the street segments were used, and the percentage of vegetation cover determined for each segment. Recognizing that other surface characteristics influence the LST, we accounted for the height to width ratio (H:W) of the urban canyons, since streets with a high H:W tend to provide more shade during the day resulting in a lower mean canyon LST. The H:W was calculated by determining the nearest distance from each street centreline record to the land parcel on each side of the street in order to establish a buffer distance. Building heights were determined from LiDAR data to calculate a mean H:W ratio for each urban canyon segment. Most of the streets in the AOI are very wide with a low H:W. The canyon segments were separated into four groups by H:W (<0.2; 0.2–0.3, 0.3–0.6, >0.6; which resulted in a similar frequency) and the linear regression coefficient was compared between vegetation cover and mean canyon LST for each group.

2.10. LST and air temperature relations

To compare T_a observed from the short transect within the CoPP with LST, a defined area of land surface influence (or 'footprint') on T_a at the street-scale needs to be attributed. This is challenging because T_a is influenced by not only adjacent surfaces, but the geometry of the landscape, wind direction and the local background meteorological conditions (Coutts et al., 2015), while LST represents surface radiative and thermodynamic properties (Voogt and Oke, 2003). Here, circular buffers of radius sizes 15, 30, 60 and 120 m were placed around each transect point to calculate a corresponding mean LST. Vegetation cover within each circular buffer was also calculated. For the west to south-east transect across Melbourne each transect point was compared with the corresponding 1 km resolution MODIS LST and NDVI (aggregated to 1 km).

3. Results and discussion

3.1. Identifying neighbourhood- and street-scale hotspots

The VHR TIR data for the entire CoPP are presented in Fig. 4 for both day and night. Such images are an excellent tool for communicating the influence of surface types on the urban climate to planners, councillors and the public. However, it was difficult to clearly and rapidly identify hotspots from such high resolution imagery. The aggregation approach however meant hotspots could be rapidly identified (Fig. 5). Neighbourhoods that were hotspots during the day were not necessarily hotspots at night, demonstrating the importance of surface radiative and thermodynamic properties on LST and that areas that heat rapidly during the day may actually cool relatively rapidly at night. This highlights the need for urban planners to consider *when* they want to provide heat mitigation (during the day and/or night), in addition to *where*. In both Figs. 4 and 5, the Albert Park area on the north-east side of the municipality where there is a large lake surrounded by well-watered open green space including parklands, sports fields and a golf course showed the coolest LST during both the day and night. In contrast, neighbourhoods with the greatest amounts of impervious surface cover (asphalt, concrete, buildings) tended to show the highest mean LST.

Considering the street-scale, the 'South Melbourne Central' area was chosen for more detailed analysis (see Section 2.8) (Fig. 6). Streets showing high LST during the day were associated with impervious surfaces such as rooftops, carparks and roads that were exposed to large amounts of solar radiation, and dry unirrigated grass which could

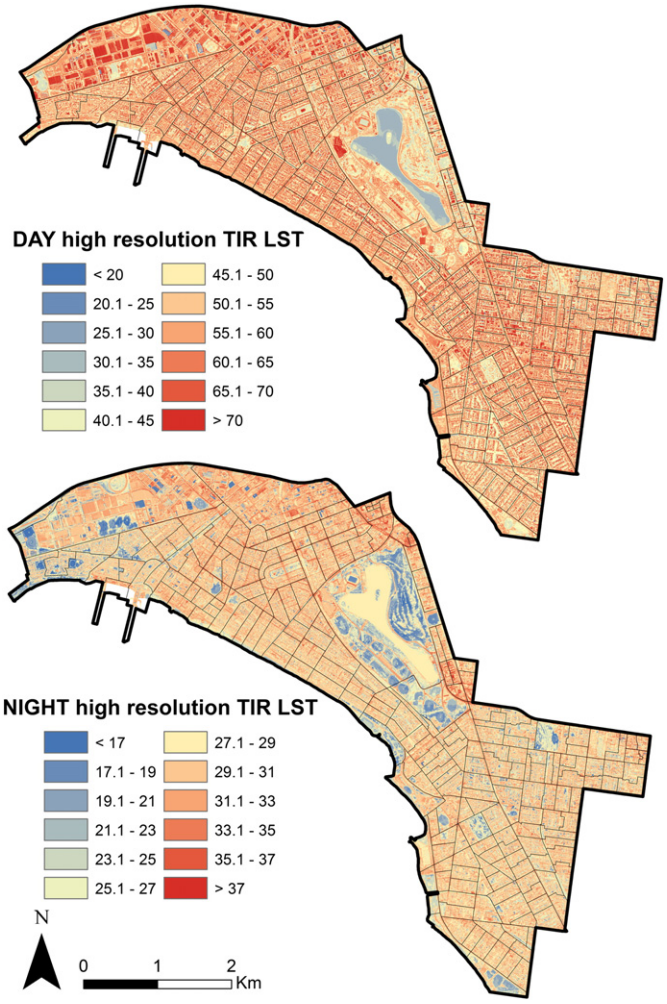

Fig. 4. VHR TIR remote sensing data (°C) for the City of Port Phillip during the day and night on 25 (26) February 2012 during warm summertime conditions. Daytime and night time scales are different. Boundaries are census statistical areas.

display LST as high as impervious surfaces. Irrigated grass, tree canopies and some rooftops showed low LST due to evapotranspiration or differences in surface radiative and thermodynamic properties. Surfaces that were shaded by buildings or trees were also cooler. At night, streets with large amounts of impervious surfaces remained warm, while pervious surfaces including un-irrigated grass cooled rapidly. The VHR TIR data can be used to identify locations where some form of heat mitigation treatment may be needed, such as where to plant street trees to provide shade or where irrigation could be used to reduce daytime LST. This approach does provide a good starting point from which to prioritise and target further investigation and site visits.

While VHR TIR data can help identify surfaces with high LST at the point in time of data capture, there are several limitations in the use of the data. Errors can arise during data collection and post-processing that compromise data quality. The atmospheric and emissivity corrections were only as good as the quality of the land surface classification, which also relied on the quality of auxiliary datasets, and literature based emissivity values. Small misalignments in datasets, image sections that are off-nadir, different shadow patterns, and changes in land cover in the years between image capture led to small errors in the 0.5 m classification and hence the derived LST. Further, no attempt was made to account for the effective thermal anisotropy of the urban surface. The TIR sensor appeared unable to capture the LST of a small number of rooftops with extremely low emissivity and our emissivity correction approach could not resolve this. Unfortunately, while LST is

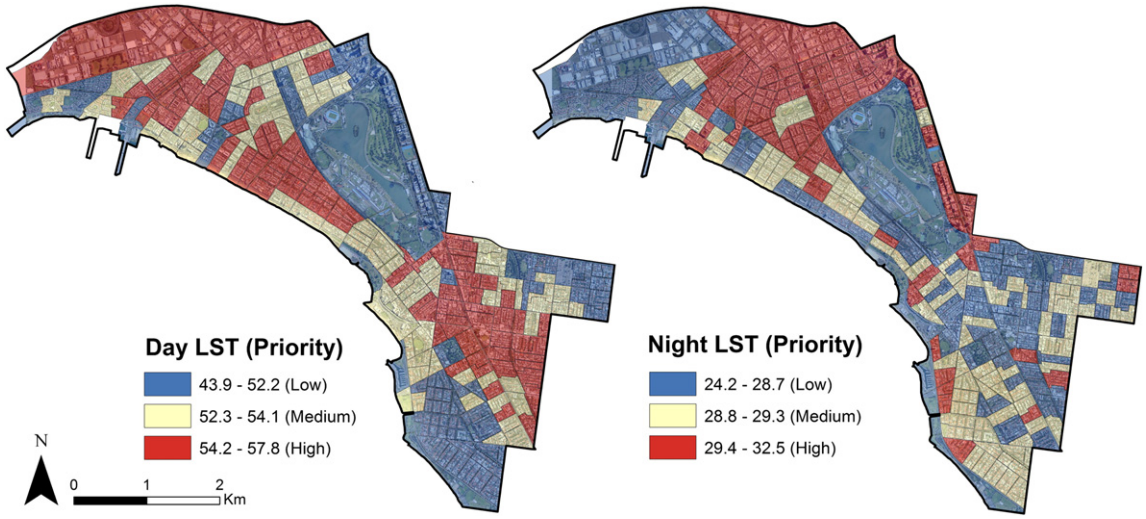

Fig. 5. Neighbourhood-scale hotspots during the day and night in the CoPP derived from the VHR TIR remote sensing data (°C), by aggregating LST for statistical areas and categorizing into three classes of priority for urban greening: Low, Medium and High (using quantile classification).

provided at very high resolutions, the data do not allow identification of radiative and thermodynamic processes driving LST (e.g. material properties, albedo, soil type, water content). Therefore, a site visit is likely required to observe what might be specifically driving the development of a high LST.

Without the necessary corrections and a thorough understanding of what the data represents, there is a risk of misinterpretation by stakeholders and the public. This is evident from the practice of asserting the energy efficiency (heat loss) of a building directly from the rooftop LST alone as attempted by different municipalities in numerous countries (e.g. Worcestershire City Council, 2015). The LST of rooftops will vary according to their material types (and thermodynamic properties), slopes, albedos, emissivities, the amount of insulation and diurnal surface net radiation that they have, and may have very little to do with the overall energy efficiency of that building, usage or occupancy, especially when the whole building envelope is considered. This practice becomes even more concerning if emissivity corrections are not undertaken at all, as a roof with low emissivity will appear cool but in fact may be performing quite poorly in terms of energy efficiency. Building walls would also need to be considered in any building energy assessment, in which case complete surface temperatures determined from various sensor view angles would be needed. In summary, VHR TIR remote sensing can be used to map detailed LST, but special care must be taken when interpreting the data, especially for rooftops. These limitations (and others) will be discussed further in relation to the use of VHR TIR remote sensing to inform urban greening (Section 3.5).

To explore the street-scale variations in LST, we considered the prioritization approach of Norton et al. (2015) which provides a prioritization hierarchy to improve pedestrian human thermal comfort based on geometry and building shade and applied it at the scale of the street canyon. This was done by considering the defined street segments (Fig. 7). Again, areas that showed high LST during the day were not necessarily the hottest at night. At this street-scale, there are a wide range of surface characteristics that influence the LST of the urban canyon. Vegetation cover, street width and orientation, building height, land surface materials and shortwave reflectance will all influence the LST. The influence of vegetation and height to width ratio (H:W) on the LST in Fig. 7 are explored further in Section 3.2. Isolating the drivers of high LST in urban canyons is difficult at this scale and LST is highly variable both spatially and temporally, but overall, wide and shallow streets with little vegetation cover and shade showed high LST during the day. Once an urban canyon has been identified for greening interventions, site visits are likely needed to ascertain appropriate heat mitigation approaches.

3.2. The influence of vegetation on land surface temperatures

Vegetation cover is a key factor in modifying the urban surface energy balance and the resulting climate. We explored the influence of vegetation cover on LST during the February 2012 heatwave, when clear skies and high air temperature led to intense surface heating (Fig. 8a). During the day, there was a linear relation between daytime LST and vegetation cover where for a 10% increase in vegetation cover, there was a 1.2 °C reduction in LST. Similar reductions in LST have been observed using satellite remote sensing data. For instance, from Landsat TM and Landsat ETM data, Klok et al. (2012) established that for a 10% increase in the amount of green area, there was a 1.3 °C reduction in LST in Rotterdam, Netherlands. At night, reductions in LST were better described by a polynomial relationship where reductions in LST were small when vegetation cover increased in areas of greater amounts of imperviousness (e.g. <30% vegetation cover). As vegetation cover increased above around 30%, night time LST reductions became larger.

While the reduction in LST with increasing vegetation cover was evident across the CoPP, when considering the outdoor thermal environment, it is at the street level where greening interventions are likely to be felt. The high resolution TIR data allowed for an analysis of vegetation cover and its role in reducing LST within urban canyons. For the AOI and associated urban canyon segments defined earlier (Fig. 7), the percent vegetation cover was calculated and compared with the mean canyon LST (the average LST of each segment) for both day and night. Results show that as vegetation cover increased, mean canyon LST reduced during both the day and night, particularly in wide, open streets where H:W < 0.6 (Fig. 8b). We found that when H:W > 0.6, the rate of LST reduction at ground level within the urban canyons was diminished, and was statistically significantly different from the categories where H:W < 0.6. This suggests that within more built up urban canyons with higher H:W and hence greater building shade, vegetation cover is less effective in reducing mean canyon LST, so vegetation should be prioritized for wide, open streets. Where H:W are higher, focus should instead be on rooftop interventions (e.g. green or reflective roofs). This aligns with the street scale prioritization hierarchy of Norton et al. (2015). This analysis demonstrates the benefits of increasing vegetation cover, yet the variability in Fig. 8b highlights the role that other surface features like the type and shortwave reflectance of surface

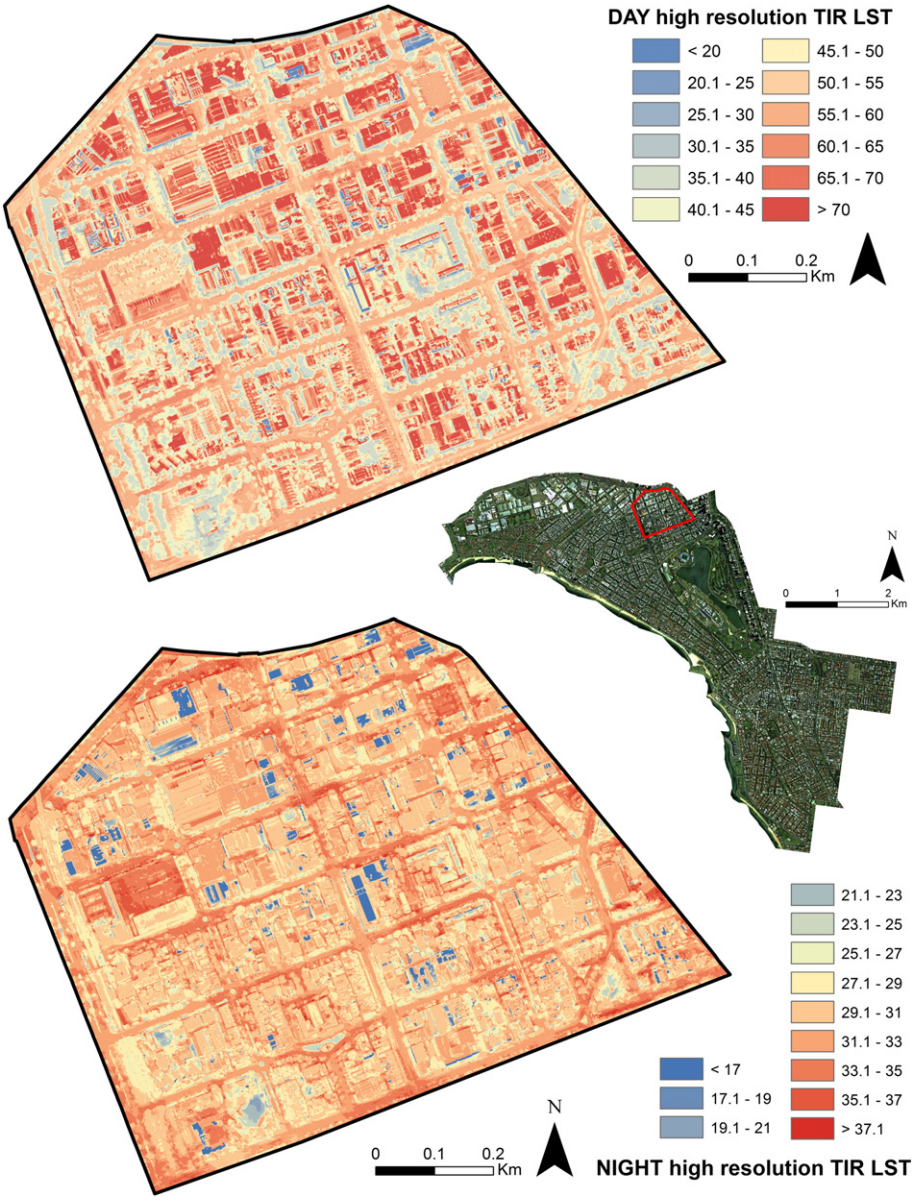

Fig. 6. VHR TIR derived LST (°C) for 'South Melbourne Central' during the day and night and its location within the City of Port Phillip. Daytime and night time scales are different.

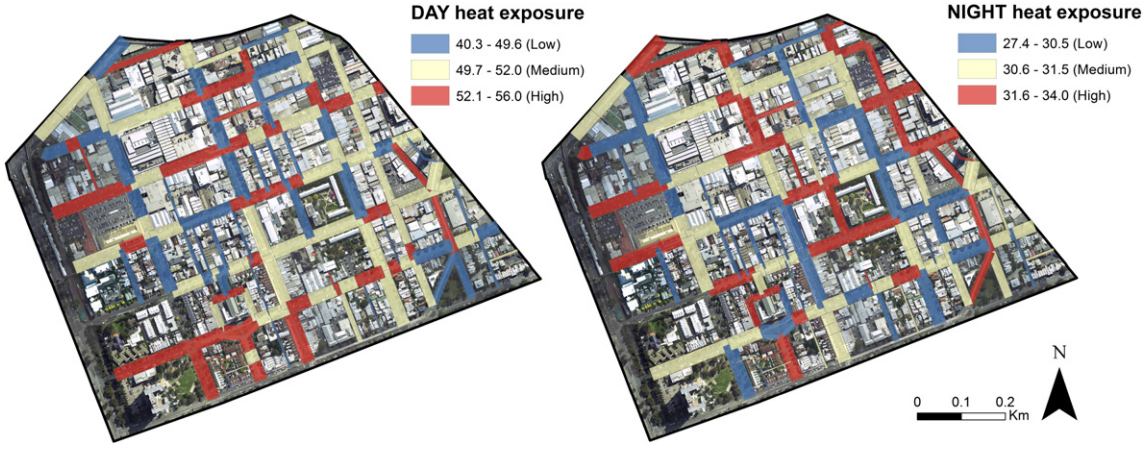

Fig. 7. Street-scale hotspots during the day and night in the area of interest derived from the VHR TIR remote sensing data, by averaging LST for urban canyon segments, and categorizing into three classes of priority for urban greening: Low, Medium and High (using quantile classification).

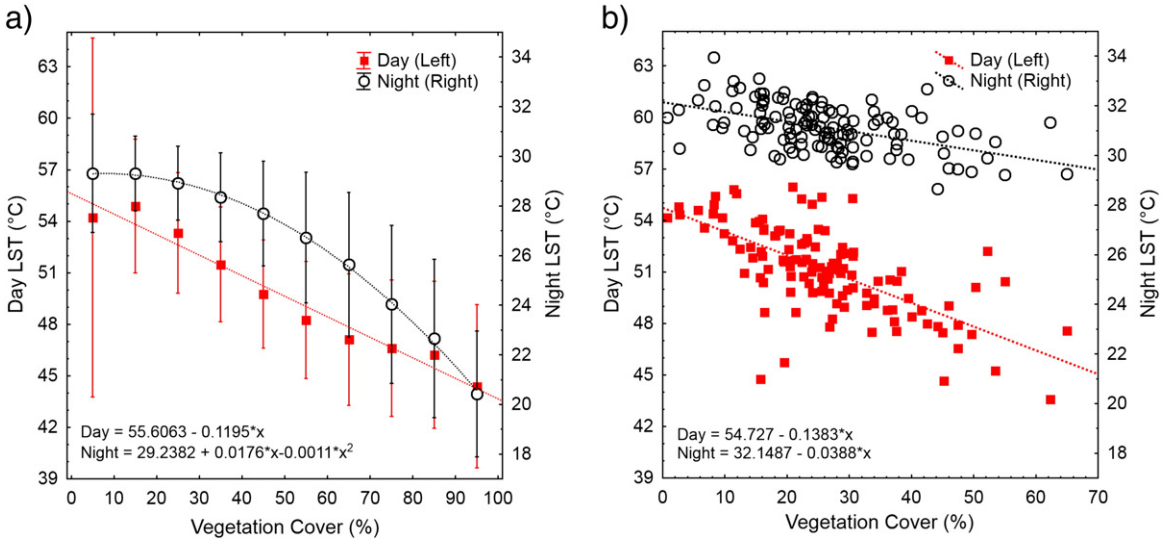

Fig. 8. Relations between vegetation cover and land surface temperature during the day and night for a) VHR TIR LST and vegetation cover aggregated to 30 m (error bars are standard deviation); and b) mean canyon LST and vegetation cover when H:W < 0.6.

materials may have on LST, which should also be tackled as part of a mix of approaches for mitigating urban heat during heatwaves.

3.3. Relations between land surface temperature and air temperature

Using TIR remote sensing as a tool to reveal hotspots and inform planning decisions to create more thermally comfortable urban environments relies on the assumption that spatial patterns in T_a are similar to patterns in LST. A T_a transect within the CoPP (Fig. 2) was conducted during the night time flight to explore similarities with the VHR TIR data. Fig. 9 compares the T_a and LST (30 m buffer) along the CoPP transect, and the total percent vegetation cover (30 m buffer) for each point. The LST was highly variable, so a six-point moving average (representing 1 min of the T_a transect) was also included, recognizing that T_a is influenced by turbulence and mixing. Fig. 9 also presents these data spatially across the CoPP, with T_a given for each measurement point along the transect and overlain on the VHR TIR data (aggregated to the statistical areas as in Fig. 5). T_a varied by up to 3.1 °C along the transect with the highest T_a occurring at the highly built up Bay Street residential and commercial zone in Port Melbourne (around point 130). The moving average of LST varied by up to around 10 °C.

Patterns in T_a broadly align with patterns in LST. Results showed that for buffer sizes (around each transect point) of 30 m and above, the relationship between LST and T_a was statistically significant ($p < 0.05$), but the correlation was weak, although it did strengthen slightly as the buffer size increased (correlation coefficient of $r = 0.21$ at 30 m and $r = 0.27$ at 120 m). This suggests that there was not a strong relationship between LST and T_a at very high resolutions (e.g. <30 m), but as the resolution of the TIR data reduces (e.g. >30 m), areas of high LST and hotspots are more likely to be co-located. LST also showed a statistically significant correlation with vegetation cover at 30 m of $r = -0.55$. There were some instances however along the transect where the relationship became decoupled (a disconnection between LST and T_a); particularly in more open areas where T_a appeared to be influenced by

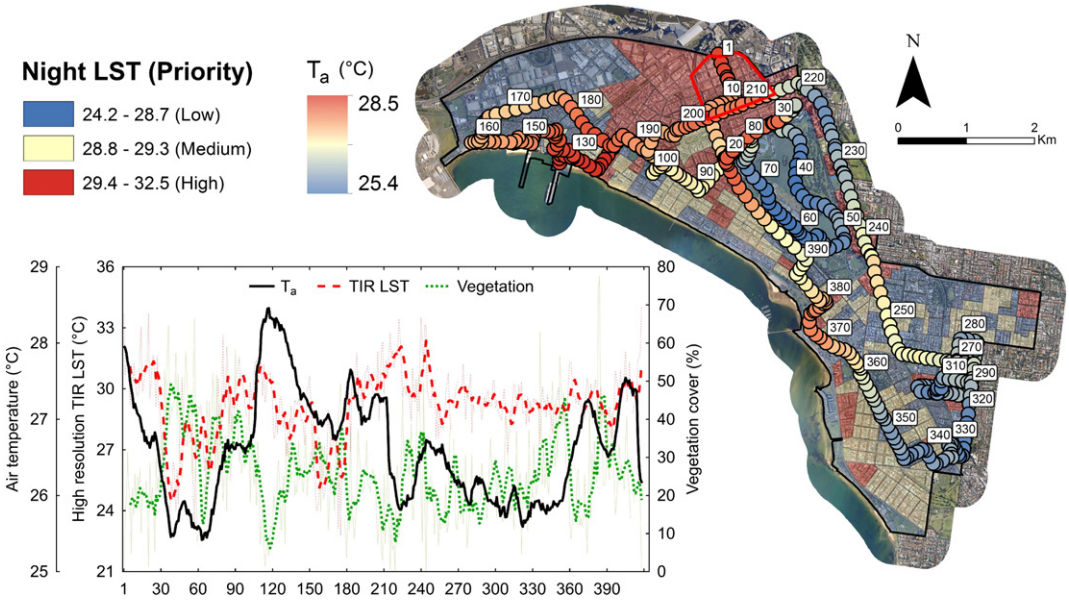

Fig. 9. Air temperature transect (circles) conducted in the City of Port Phillip at 1:00 26 February 2012 (night of the 25 February 2012), overlain on the statistical areas and their prioritization levels. A profile comparison of air temperature, vegetation cover (from the land surface classification) and LST (using a 6 point moving average representing a 1 min temporal average and 30 m buffer) is also given. The x-axis corresponds to the points (boxes) on the map.

advection of micro- and local-scale air masses. At points 220–240, T_a reduced while LST increased; this was hypothesised to be a result of cool air being advected from large parklands to the north-east of the CoPP under the observed northerly wind direction at the time. Also in this area, there are several tall buildings, so a disconnection may exist between the rooftop level LST and low-level advected cool air at the street level in what Roth et al. (1989) described as a methodological mismatch. These findings suggest that hotspots should only be attempted to be identified using TIR data at resolutions >30 m. This is because canopy layer T_a depends on the flux divergence in the air volume, including advection, as well as the surface energy balance (which controls surface temperature) of a variety of urban surfaces (Roth et al., 1989). High resolution TIR remote sensing on the other hand captures the LST of individual surface types.

Given the influence of scale on the relations between LST and T_a, a simple comparison at the city-scale was conducted for the same night using 1 km MODIS data (Fig. 3) and the west to south-east T_a transect (Fig. 2). From this cross-city transect, results showed similar patterns between LST and T_a (Fig. 10) and the correlation was statically significant ($p < 0.05$) with a correlation coefficient of $r = 0.81$ suggesting LST may act as a good proxy for T_a at this city-scale and time of day (night). Further, Fig. 3 showed the presence of a night time surface UHI, and that many of the areas with a high LST at night corresponded with areas with a low NDVI (a statistically significant ($p < 0.05$) correlation of $r = -0.41$). Green areas, particularly those with large open grassy areas, cool down rapidly at night compared to built-up impervious areas that have a high heat capacity. While there is a significant relationship between NDVI and LST at this city-scale, NDVI is only an indicator of the extent of vegetation cover and the health of the biomass, and is not a direct measure of the vegetation cover. It should be noted that there is somewhat of a mismatch in scale between these two data sources, as the MODIS LST data (1 km) is representative of the local-scale, while the T_a data captured along the roadways is more representative of the micro-scale (e.g. tens to hundreds of metres). This city-scale comparison also lacks multi-temporal data, and further research should be undertaken to examine these vegetation, LST and T_a relations across diverse temporal periods.

Tomlinson et al. (2011) notes that *"… a significant research gap still exists which is the quantification of the relationship between measured air temperatures and remotely sensed LST data."* The data presented here highlights several limitations in the assumption that patterns in LST are similar to patterns in T_a, and this needs to be acknowledged. Previous research indicates that LST and T_a relations tend to be stronger under more stable atmospheric conditions and hence are stronger at night when micro-scale advection is reduced, but are weaker under higher wind velocities when they become decoupled (Stoll and Brazel, 1992; Unger et al., 2010). The CoPP transect was not completed during the day, so it is unknown if the patterns were similar at this time, although the ability to estimate canopy layer T_a based on satellite derived LST has been shown to depend on the time of day (Keramitsoglou et al., 2016). Further, the data collected here represents only one point in time under ideal meteorological conditions, and therefore lacks any multi-temporal comparisons.

Multiple thermal images and transects should be captured/conducted to further test the assumption and more strongly define appropriate resolutions at which areas of high LST can confidently claim to represent hotspots. We found that the LST from the VHR TIR was generally higher than T_a, which is in contrast with the cross-city transect (Fig. 10) where LST from MODIS were much lower than T_a. The 30 m buffers of the VHR TIR data for the CoPP transect centre on, and encompass much of the road surface within the canyon, so LST was high (Fig. 9). In contrast, the coarser resolution of the MODIS satellite data means each pixel incorporates a broader range of land cover types (e.g. grass, roads, buildings) so the differences in LST between individual surface types are averaged. This highlights that empirical relationships between LST and T_a will vary with the scale of the data. As Klok et al. (2012) acknowledge in their comparison of Landsat based LST and T_a from local weather stations in the city of Rotterdam, because of different surface and meteorological drivers, T_a cannot be based on such a correlation. However *"the spatial variation in surface temperature is a strong indicator for variations in air temperature"* (Klok et al., 2012) (pg. 27).

We have shown here that relations between LST and T_a tend to strengthen as that spatial resolution of the TIR remote sensing data coarsens. According to Stoll and Brazel (1992) regarding air-surface temperature relations in urban environments, a more appropriate scale of analysis for urban climate research is a resolution of around 250 m. This actually aligns well with the approach applied here for neighbourhood-scale hotspot identification where the average size of the statistical areas were 0.09 km^2. In contrast, un-aggregated VHR TIR data (<30 m) should not be as a proxy for hotspots. A more suitable application of VHR TIR data is for identifying locations where pedestrians are likely to be experiencing relatively poor human thermal comfort during the day as a result of high levels of solar exposure and high LST (at the time of the image capture). High radiant loads increases mean radiant temperature, which has been shown to be the dominant driver of human thermal comfort in warm, sunny conditions (Coutts et al., 2015).

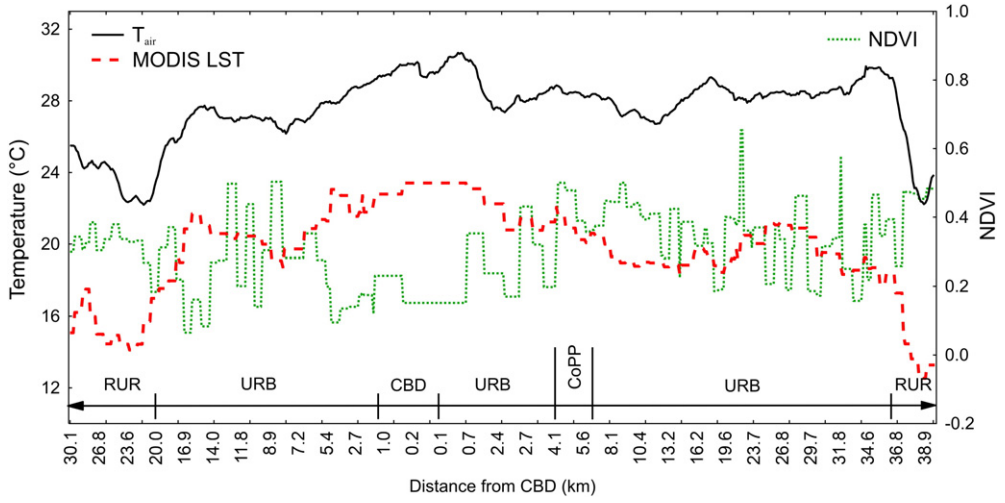

Fig. 10. Transect from west to south-east across metropolitan Melbourne presenting air temperature from an automobile transect at 01:00 on 26 February 2012, LST from MODIS at 1 km resolution, and Normalized Difference Vegetation Index (NDVI) aggregated to 1 km resolution (right axis).

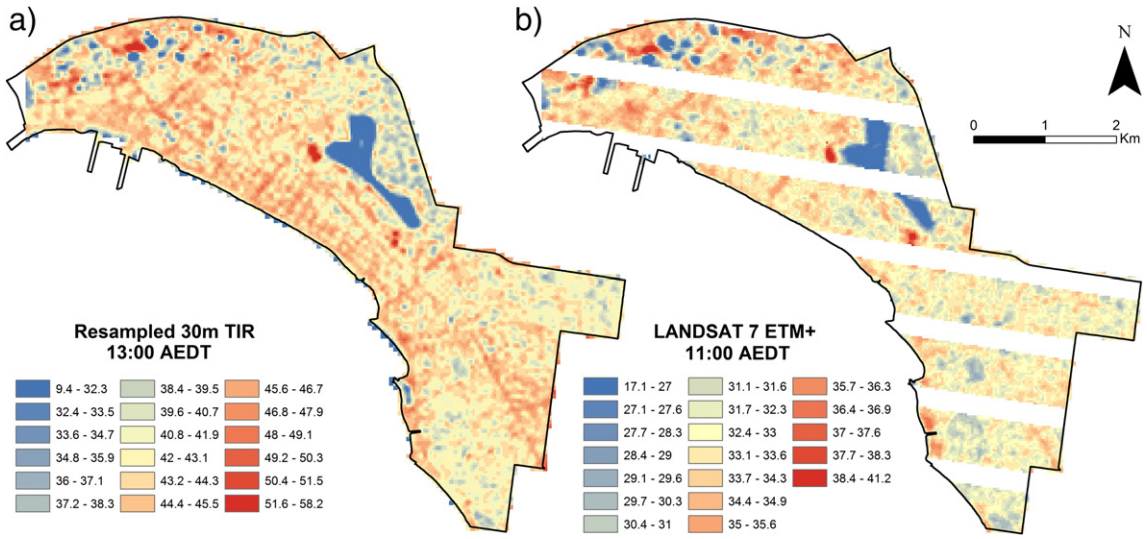

Fig. 11. Comparison of patterns in surface brightness temperature throughout the City of Port Phillip on 25 February 2012 between a) daytime (13:00) VHR TIR remote sensing data (radiometric data aggregated to 60 m and resampled to 30 m using cubic convolution); and b) the daytime (11:00) Landsat 7 ETM+ thermal image. The white areas of the Landsat 7 image are missing data.

3.4. Correlation between Landsat and VHR TIR data

Fig. 11 presents a unique comparison of the brightness temperature of two images on the same day: a) 30 m resolution VHR TIR remote sensing data; and b) 30 m Landsat 7 ETM+ data. While the Landsat 7 ETM+ data were acquired for the same day, it represents the LST approximately 2 h prior to that derived from the VHR TIR data. Landsat 7 ETM+ is not representative of the peak daytime surface heating, and different surface types and materials, urban geometries, and surface moisture conditions will drive varying surface heating and cooling rates throughout the day. Despite this, the patterns of relatively warmer and cooler areas were similar between images and the data were spatially correlated with an r^2 of 0.73 (Fig. 12). Therefore, despite the lower LST measured by Landsat at the time of image acquisition, Landsat can be used satisfactorily to identify areas of high LST and at this scale, is likely to represent the location of hotspots well. Further, users of Landsat imagery can have greater confidence in the LST values, as image processing follows standardized and well documented procedures, and the coarser resolution precludes the need for the detailed emissivity corrections (unlike the VHR TIR data). Drawing on multi-temporal imagery and modelling approaches could also help to better document time-varying LST. Landsat can be effectively used to identify hotspots at the neighbourhood-scale and provide sufficient information to inform urban greening interventions for urban heat mitigation.

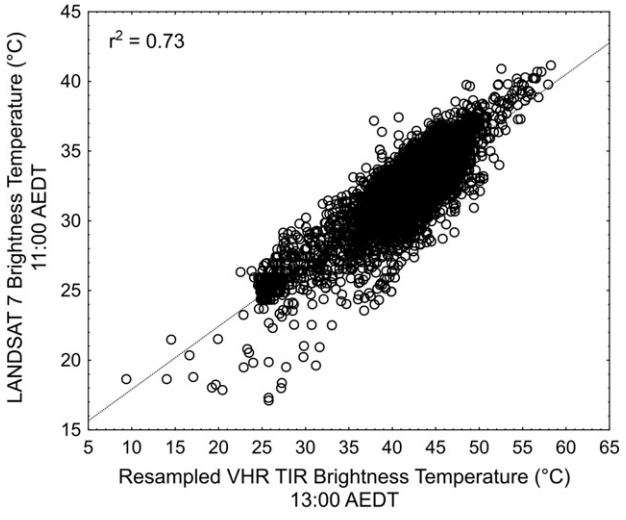

Fig. 12. Comparison between the brightness temperature of the resampled 30 m VHR TIR data at 13:00 AEDT and the 30 m Landsat 7 ETM+ at 11:00 AEDT on 25 February 2012. Land surface temperatures are not expected to match due to different capture times, however the data are spatially correlated.

3.5. Practical application of VHR TIR remote sensing in urban planning

There are a wide range of TIR remote sensing products available that could be applied in the context of urban planning and heat mitigation. To reiterate, the objective of the local municipality was to use VHR TIR data to identify hotspots (areas of relatively high T_a) that could be mitigated with increased tree canopy cover. So, can VHR TIR remote sensing be used to identify hotspots at the neighbourhood-scale and the street-scale? Under the assumption that areas of relatively high LST coincide with the areas of relatively high T_a, TIR data at very high resolutions cannot identify hotspots because this assumption does not hold. However, if the data were aggregated to a coarser spatial scale, then the assumption is more reliable meaning aggregated LST from VHR TIR data can be used to identify neighbourhood-scale hotspots. This finding highlights the importance of first identifying the scale at which users are working. For our context of municipal-wide hotspot identification, the application of VHR TIR data is highly questionable and in practice, cost-benefit analysis of the acquisition of such data leave the approach unjustifiable. Instead, a coarser resolution approach such as Landsat will suffice (Tomlinson et al., 2011).

Landsat TIR remote sensing presents an attractive alternative as it is more accessible, cheaper to acquire, has established routines for data processing, has a variety of image capture dates, and provides accessible auxiliary datasets such as NDVI. The use of satellite based approaches mean that temporal variations in LST can be accounted for by acquiring several images and quantifying the variability of hotspots (in terms of LST). Because of the more established approaches for processing Landsat imagery, there is a greater likelihood that the full suite of image corrections will be undertaken, minimising the risk of misinterpretation by stakeholders. Disadvantages of Landsat data are that the time of acquisition varies according to your latitude and longitude (11:00 am AEDT for Melbourne, Australia) which does not coincide with the optimum times suggested for urban heat analysis (Table 1).

However, as demonstrated here, the daytime patterns in LST derived from Landsat and those derived from the aggregation of the VHR TIR data were similar (Figs. 11 and 12) meaning Landsat can confidently be used for daytime hotspot identification. Other limitations of Landsat however are the lack of nocturnal imagery and the 16-day revisit time that limits its temporal scale (Tomlinson et al., 2011).

From this study we conclude that VHR TIR derived LST are more relevant in designing urban spaces for improved human thermal comfort in an AOI by identifying areas of high solar radiation, urban designs that are susceptible to high LST, and where trees and irrigation can be provided to promote shading and evapotranspirative cooling. While there may be a role for VHR TIR, the limitations of the data must be recognized. We found that in the case of VHR airborne TIR remote sensing that the collection, evaluation and post-processing of the data to achieve a high quality product was difficult and expensive. Without the supporting funding provided in this collaborative project, the atmospheric and emissivity corrections were unlikely to have been feasible due to lack of necessary image processing skills and/or additional costs. Without these corrections, the TIR data simply represents the surface brightness temperature. The value of the VHR TIR data relied heavily on the ability of the service provider to deliver a high quality product using a thermal camera that could accurately capture LST. The funding and collaborative nature of this project allowed for a ground based evaluation of the thermal image and is unlikely to be undertaken in other TIR capture situations. The value of the TIR data also relies on capturing LST during meteorological conditions that support high quality data (Table 1). As such, there is a limited window of opportunity, and it can easily be missed.

While ideal conditions may be successfully captured, an important limitation is that the data are temporally poor, representing only a snapshot in time that neglects the variations in LST resulting from shading, different moisture conditions, and variations in meteorology. In reality, high LST will change location and intensity over weeks, days and even hours, especially at such high resolutions. As such, multiple images should be captured to elucidate such temporal changes in LST. Fixed cameras can allow a comparison between multi-temporal imagery (Meier et al., 2010). Auxiliary datasets that can support emissivity corrections and interpretation, such as high resolution aerial photography, hyperspectral data and LiDAR should ideally be captured at the same time and be of equal high quality as the thermal imagery to reduce misalignment between data sources, and issues resulting from different capture times (e.g. differential shading and data collection dates) and days (e.g. varying soil moisture status). Alternatively, hyperspectral imagery with multiple bands in the thermal spectral range would allow the application of Temperature – Emissivity Separation algorithms (Heshun et al., 2011). Without high quality, corrected data, and an understanding of what the data actually represents, there is a risk of misinterpretation that may lead to incorrectly identifying landscape features (particularly rooftops) that enhance or mitigate urban heat and thus misinform policy. For instance, if there is a large amount of variation in emissivity, one rooftop may appear cooler than another when in fact the actual LST is similar, but the emissivity is different (Artis and Carnahan, 1982).

4. Conclusions

There is an important role for TIR remote sensing at a range of scales that can help address the issue of urban heat through urban planning and design. VHR TIR remote sensing can be used to identify areas of high LST at the time of capture. However, in order to assume that areas of high LST are co-located with hotspots and act as a proxy for areas of high air temperature, the data must be at a suitably coarse spatial scale, with a resolution >30 m. As the spatial resolution of TIR remote sensing data becomes coarser, the assumption of co-location strengthens. In this study, the VHR TIR data was aggregated to identify neighbourhood and street-scale hotspots. At very high resolutions (<30 m), it cannot be assumed that areas of high LST identified through VHR TIR remote sensing are co-located with hotspots. Rather, such data are more suited to the identification of areas of poor human thermal comfort resulting from high solar exposure (limited shade). Either way, the data can be used to inform urban planning and design decisions. Such data can be used in unison with population vulnerability data and population activity data to prioritise locations for urban greening and improve the cost effectiveness of investment (Norton et al., 2015).

TIR remote sensing is but one of a suite of tools that could be employed in urban planning when appropriately used. Other tools such as urban climate modelling at a range of scales could also support decision making, with the benefit of being able to directly model air temperatures without relying on assumed relations between LST and T_a. Urban climate modelling can also be used to explore and assess a range of urban greening and development scenarios, and there are a range of urban climate models available (and in development), including several micro-scale radiation models such as SOLWEIG (Lindberg and Grimmond, 2011). Tools need to be user friendly and readily available for planners to meet and assess their own particular circumstances. As Ren et al. (2012) states there is still a huge gap between the work of spatial planners and the work of climate scientists, but TIR remote sensing could be one approach to bridge this gap as demonstrated here. Local authorities require information and sometimes guidance to plan urban greening interventions to improve the local climate and, to that end, TIR remote sensing is a useful product for mapping hotspots. The data demonstrated that increasing vegetation cover leads to a reduction in LST, especially in wide open streets during the day (e.g. where H:W < 0.6).

A key finding was the need for users to clearly define the scale at which they intend to apply remotely sensed TIR data, as this will dictate the appropriate data source(s). If the identification of hotspots in local municipalities is the objective in order to prioritise neighbourhoods for heat mitigation, then a satellite product such as Landsat is suitable. Landsat provides excellent spatial coverage, is easily accessible, routinely captured, processes for corrections are well documented, and a number of supporting datasets to assist in interpretation and planning such as NDVI are available at equivalent resolutions. Keramitsoglou et al. (2012) also conclude that satellite remote sensing can help city planners by providing insight into local scale hotspots. White-Newsome et al. (2013) suggest several ways in which remote sensing data could be better integrated into public health practice and its relevance for assessing areas of high LST including: increased frequency of data capture; more accessible processed data; and more research to derive a more precise LST useful in planning for heatwaves. If a particular time of the day or night is required for planning and design purposes, then airborne TIR remote sensing can be used, but in contrast with the White-Newsome et al. (2013) suggestion of higher resolution (10–15 m), we contend that resolution need not be so high. Airborne TIR remote sensing could be undertaken at a height that delivers an at-surface resolution equivalent to Landsat (60 m resampled to 30 m) which would reduce the flying time (and costs) and can then be complemented with Landsat products such as NDVI. Further, synergistic methods are being developed that attempt to downscale low resolution thermal imagery using information on land surface cover at a higher resolution to improve spatio-temporal availability of LST estimates (Mitraka et al., 2015). If the scale at which users intend to apply TIR data is the streetscape or public spaces (possibly identified via Landsat as having high LST and hence require some intervention), then VHR TIR data can provide some additional information and could even be achieved using unmanned automated vehicles (UAV). This can help guide design decisions to improve human thermal comfort such as where to locate street trees to provide shade, which road surface materials require modification to reduce LST, and what urban design arrangements (e.g. street geometry and orientation) tend to support higher surface temperatures.

Acknowledgements

This work was carried out with financial support from the State of Victoria through the Victorian Centre for Climate Change Adaptation Research (VCCCAR). Funding was also provided through the Cooperative Research Centre (CRC) for Water Sensitive Cities. Monash University provides research into the CRC for Water Sensitive Cities through the Monash Water for Liveability Centre. We would like to acknowledge Shobhit Chandra for project managing the capture of the thermal imagery, Jason Beringer for assistance in data collection, and both Lalitha Ramachandran and Rizwan Haque at the City of Port Phillip for partnering in the research, providing data, and their assistance in the project. We would like to thank three anonymous reviewers who provided excellent feedback that helped improve the quality of the manuscript.

Appendix A

Considering Eq. (1), taking the total observed radiance received at the sensor $L(h,\theta)$ and subtracting the atmospheric radiance component (L_a), the 'remaining' radiance received at the sensor $[\tau(h,\theta)\varepsilon L_0 + \tau(h,\theta)(1-\varepsilon)L_{sky}]$ must be apportioned into either surface radiance (L_0) or reflected radiance (L_{sky}). This apportioning is determined by the emissivity (Eq. (1)). We developed a linear relationship for roofs between emissivity and this 'remaining' radiance based on low and high roof radiance values.

To determine an emissivity value for roofs with low radiances, we drew on the ground based evaluation sensor located on the metal roof. This roof presented amongst the lowest radiance values from the entire TIR data and the ground evaluation site for the metal roof gave a surface radiance value of $L = 291.6\ \mathrm{W\ m^{-2}}$ at night. Using Eq. (1), we determined the surface radiance (L_0) of the metal roof using the ground evaluation data, but adjusted the emissivity until the resulting LST was at its maximum (10.0 °C), which gave an emissivity value of $\varepsilon = 0.5$. We then needed to establish an emissivity value for roofs with higher radiances, in this case tiled roofs. From the literature, tiled roofs have an emissivity of 0.9 (Oke, 1987) and so we sought to find a corresponding radiance value for tiled roofs. From the night time TIR data we determined an average radiance value (L) for several tiled roofs in the CoPP that were clearly identifiable from aerial imagery, which gave $L = 422.3\ \mathrm{W\ m^{-2}}$. We then assumed a linear relationship between ε and $L(h,\theta) - L_a$ at these radiances (where night time $L_a = 51.6\ \mathrm{W\ m^{-2}}$) to apportion the 'remaining' longwave radiation based on emissivity and determine the surface radiance (L_0), where:

$$\varepsilon = 0.0031 \times (L(h,\theta) - L_a) - 0.2344 \quad \text{(A1)}$$

Because rooftops can comprise tiled roofs, metal roofs, and concrete roofs, we set the maximum emissivity at 0.94 (concrete). This approach gave very reasonable and realistic values for the LST of rooftops. The emissivity data (Fig. 1b) developed using the night time TIR data was then applied to the daytime TIR data in the calculation of daytime LST. Table 3 presents a comparison of the final LST for the surfaces observed at the ground evaluation sites. For the metal roof, applying the varying emissivity approach to the TIR data resulted in a good agreement in the calculation of the LST (12.2 °C compared to 10.0 °C for the ground based sensor). Daytime LST values of the metal roof were also relatively similar (51.0 °C for the TIR data and 50.0 °C for the ground based sensor), so $\varepsilon = 0.5$ was set as the minimum emissivity for rooftops. We also set the surface radiance at a minimum of $L = 290\ \mathrm{W\ m^{-2}}$ because when Eq. (1) was applied below this value, LST declined rapidly giving unrealistic or null values.

References

Aniello, C., Morgan, K., Busbey, A., Newland, L., 1995. Mapping micro-urban heat islands using LANDSAT TM and a GIS. Comput. Geosci. 21, 965–969.
Artis, D.A., Carnahan, W.H., 1982. Survey of emissivity variability in thermography of urban areas. Remote Sens. Environ. 12, 313–329.
Arya, P.S., 2001. Introduction to Micrometeorology. Academic Press, Great Britain.
Bärring, L., Mattsson, J.O., Lindqvist, S., 1985. Canyon geometry, street temperatures and urban heat island in Malmö, Sweden. J. Climatol. 5, 433–444.
Berk, A., Bernstein, L.S., Robertson, D.C., 1989. MODTRAN®: A Moderate Resolution Model for LOWTRAN 7, GL-TR-89-0122, Geophysics Directorate. 01731. Phillips Laboratory, Hanscom AFB, MA (April 1989) ADA214337.
Berk, A., Acharya, P.K., Bernstein, L.S., Anderson, G.P., Chetwynd Jr., J.H., Hoke, M.L., 2000. Reformulation of the MODTRAN® Band Model for Finer Spectral Resolution," Proceedings of SPIE Vol. 4049, Orlando, Florida, (April 2000).
Bowler, D.E., Buyung-Ali, L., Knight, T.M., Pullin, A.S., 2010. Urban greening to cool towns and cities: a systematic review of the empirical evidence. Landsc. Urban Plan. 97, 147–155.
Chen, Y., Wong, N.H., 2009. Thermal impact of strategic landscaping in cities: a review. Advances in Building Energy Research 3, 237–260.
City of Port Phillip (CoPP) (2007). South Melbourne Central: Structural Plan and Implementation Strategy. http://www.portphillip.vic.gov.au/south_melbourne_central.htm Accessed January 2014.
City of Port Phillip (CoPP) (2010). Greening Port Phillip: An Urban Forest Approach. http://www.portphillip.vic.gov.au/greening_port_phillip.htm Accessed January 2014.
Coutts, A.M., Tapper, N.J., Beringer, J., Loughnan, M., Demuzere, M., 2013. Watering our cities: the capacity for water sensitive urban design to support urban cooling and improve human thermal comfort in the Australian context. Prog. Phys. Geogr. 37, 2–28.
Coutts, A.M., White, E., Tapper, N.J., Beringer, J., Livesley, S.J., 2015. Temperature and human thermal comfort effects of street trees across three contrasting street canyon environments. Theor. Appl. Climatol. 1–14.
Definiens, 2013. eCognition Developer 8.9 User Guide.
Dimoudi, A., Nikolopoulou, M., 2003. Vegetation in the urban environment: microclimatic analysis and benefits. Energy and Buildings 35, 69–76.
Duan, S.-B., Li, Z.-L., Tang, B.-H., Wu, H., Tang, R., Bi, Y., Zhou, G., 2014. Estimation of diurnal cycle of land surface temperature at high temporal and spatial resolution from clear-sky MODIS data. Remote Sens. 6, 3247.
ESRI, 2013. ArcGIS Desktop 10.2. Environmental Systems Research Institute, Redlands, CA.
Geiger, R., Aron, R.H., Todhunter, P., 2009. The Climate Near the Ground. Rowman & Littlefield.
Gillespie, A., Rokugawa, S., Matsunaga, T., Cothern, J.S., Hook, S., Kahle, A.B., 1998. A temperature and emissivity separation algorithm for advanced spaceborne thermal emission and reflection radiometer (ASTER) images. Geoscience and Remote Sensing, IEEE Transactions on 36, 1113–1126.
Goldbach, A., Kuttler, W., 2012. Quantification of turbulent heat fluxes for adaptation strategies within urban planning. Int. J. Climatol. n/a-n/a.
Harman, D.L., 1994. Global Physical Climatology. Academic Press, United States.
Hart, M., Sailor, D., 2009. Quantifying the influence of land-use and surface characteristics on spatial variability in the urban heat island. Theor. Appl. Climatol. 95, 397–406.
Heshun, W., Qing, X., Hua, L., Bo, Z., 2011. Temperature and emissivity separation algorithm for TASI airborne thermal hyperspectral data. Electronics, Communications and Control (ICECC), 2011 International Conference on, 9–11 Sept. 2011. pp. 1075–1078.
Honjo, T., Takakura, T., 1990. Simulation of thermal effects of urban green areas on their surrounding areas. Energy and Buildings 15, 443–446.
Keramitsoglou, I., Daglis, I.A., Amiridis, V., Chrysoulakis, N., Ceriola, G., Manunta, P., Maiheu, B., De Ridder, K., Lauwaet, D., Paganini, M., 2012. Evaluation of satellite-derived products for the characterization of the urban thermal environment. J. Appl. Remote. Sens. 6, 061704.
Keramitsoglou, I., Kiranoudis, C.T., Sismanidis, P., Zakšek, K., 2016. An online system for nowcasting satellite derived temperatures for urban areas. Remote Sens. 8, 306.
Klok, L., Zwart, S., Verhagen, H., Mauri, E., 2012. The surface heat island of Rotterdam and its relationship with urban surface characteristics. Resour. Conserv. Recycl. 64, 23–29.
Kottmeier, C., Biegert, C., Corsmeier, U., 2007. Effects of urban land use on surface temperature in berlin: case study. Journal of Urban Planning and Development 133, 128–137.
Land Processes Distributed Active Archive Centre (LP DAAC). (2014). Land Surface Temperature and Emissivity Daily L3 Global 1 km Grid SIN [Online]. Available https://lpdaac.usgs.gov/products/modis_products_table/myd11a1 Accessed 4 September 2014.
Li, X., Zhou, W., Ouyang, Z., Xu, W., Zheng, H., 2012. Spatial pattern of greenspace affects land surface temperature: Evidence from the heavily urbanized Beijing metropolitan area, China. Landsc. Ecol. 27, 887–898.
Lindberg, F., Grimmond, C., 2011. The influence of vegetation and building morphology on shadow patterns and mean radiant temperatures in urban areas: model development and evaluation. Theor. Appl. Climatol. 105, 311–323.
Lo, C.P., Quattrochi, D.A., Luvall, J.C., 1997. Application of high-resolution thermal infrared remote sensing and GIS to assess the urban heat island effect. Int. J. Remote Sens. 18, 287–304.
Loughnan, M.E., Tapper, N.J., Phan, T., Lynch, K., McInnes, J.A., 2013. A Spatial Vulnerability Analysis of Urban Populations During Extreme Heat Events in Australian Capital Cities. National Climate Change Adaptation Research Facility, Gold Coast 128 pp.
Loughner, C.P., Allen, D.J., Zhang, D.-L., Pickering, K.E., Dickerson, R.R., Landry, L., 2012. Roles of urban tree canopy and buildings in urban heat island effects: parameterization and preliminary results. J. Appl. Meteorol. Climatol. 51, 1775–1793.
Meier, F., Scherer, D., Richters, J., 2010. Determination of persistence effects in spatio-temporal patterns of upward long-wave radiation flux density from an urban courtyard by means of time-sequential thermography. Remote Sens. Environ. 114, 21–34.
Mieruch, S., Noël, S., Bovensmann, H., Burrows, J.P., 2008. Analysis of global water vapour trends from satellite measurements in the visible spectral range. Atmos. Chem. Phys. 8, 491–504.

Mitraka, Z., Chrysoulakis, N., Doxani, G., Del Frate, F., Berger, M., 2015. Urban surface temperature time series estimation at the local scale by spatial-spectral unmixing of satellite observations. Remote Sens. 7, 4139.
Morris, C.J.G., Simmonds, I., 2000. Associations between varying magnitudes of the urban heat island and the synoptic climatology in Melbourne, Australia. Int. J. Climatol. 20, 1931–1954.
Nichol, J.E., Fung, W.Y., Lam, K.-S., Wong, M.S., 2009. Urban heat island diagnosis using ASTER satellite images and 'in situ' air temperature. Atmos. Res. 94, 276–284.
Noël, S., Buchwitz, M., Burrows, J.P., 2004. First retrieval of global water vapour column amounts from SCIAMACHY measurements. Atmos. Chem. Phys. 4, 111–125.
Norton, B.A., Coutts, A.M., Livesley, S.J., Harris, R.J., Hunter, A.M., Williams, N.S.G., 2015. Planning for cooler cities: a framework to prioritise green infrastructure to mitigate high temperatures in urban landscapes. Landsc. Urban Plan. 134, 127–138.
Oke, T.R., 1987. Boundary Layer Climates. Cambridge University Press, Great Britain.
Pu, R., Gong, P., Michishita, R., Sasagawa, T., 2006. Assessment of multi-resolution and multi-sensor data for urban surface temperature retrieval. Remote Sens. Environ. 104, 211–225.
Quattrochi, D.A., Ridd, M.K., 1994. Measurement and analysis of thermal energy responses from discrete urban surfaces using remote sensing data. Int. J. Remote Sens. 15, 1991–2022.
Ren, C., Spit, T., Lenzholzer, S., Yim, H.L.S., Heusinkveld, B., Van Hove, B., Chen, L., Kupski, S., Burghardt, R., Katzschner, L., 2012. Urban climate map system for Dutch spatial planning. Int. J. Appl. Earth Obs. Geoinf. 18, 207–221.
Rogan, J., Ziemer, M., Martin, D., Ratick, S., Cuba, N., Delauer, V., 2013. The impact of tree cover loss on land surface temperature: a case study of Central Massachusetts using Landsat thematic mapper thermal data. Appl. Geogr. 45, 49–57.
Rosenzweig, C., Solecki, W.D., Cox, J., Hodges, S., Parshall, L., Lynn, B., Goldberg, R., Gaffin, S., Slosberg, R.B., Savio, P., Watson, M., Dunstan, F., 2009. Mitigating New York City's Heat Island: integrating stakeholder perspectives and scientific evaluation. Bull. Am. Meteorol. Soc. 90, 1297–1312.
Roth, M., Oke, T.R., Emery, W.J., 1989. Satellite-derived urban heat islands from three coastal cities and the utilization of such data in urban climatology. Int. J. Remote Sens. 10, 1699–1720.
Rouse, J.W., Haas, R.H., Schell, J.A., Deering, D.W., 1974. Monitoring Vegetation Systems in the Great Plains with ERTS. United States. pp. 309–317.
Saaroni, H., Ben-Dor, E., Bitan, A., Potchter, O., 2000. Spatial distribution and microscale characteristics of the urban heat island in Tel-Aviv, Israel. Landsc. Urban Plan. 48, 1–18.
Spronken-Smith, R.A., Oke, T.R., 1998. The thermal regime of urban parks in two cities with different summer climates. Int. J. Remote Sens. 19, 2085–2104.
Stoll, M.J., Brazel, A.J., 1992. Surface-air temperature relationships in the urban environment of Phoenix, Arizona. Phys. Geogr. 13, 160–179.
Tomlinson, C.J., Chapman, L., Thornes, J.E., Baker, C., 2011. Remote sensing land surface temperature for meteorology and climatology: a review. Meteorol. Appl. 18, 296–306.
Tucker, C.J., 1979. Red and photographic infrared linear combinations for monitoring vegetation. Remote Sens. Environ. 8, 127–150.
Unger, J., Gã¡L, T., Rakonczai, J., Mucsi, L., Szatmã¡Ri, J., Tobak, Z., Van Leeuwen, B., Fiala, K., 2010. Modeling of the urban heat island pattern based on the relationship between surface and air temperatures. Idojaras 114, 287–302.
United States Geological Survey (USGS) (2014). Landsat Surface Reflectance Climate Data Record [Online]. Available http://landsat.usgs.gov/CDR_LSR.php (Accessed 4 September 2014).
Voogt, J.A., 2000. Image representations of complete urban surface temperatures. Geocarto International 15, 21–32.
Voogt, J.A., Oke, T.R., 1998. Effects of urban surface geometry on remotely-sensed surface temperature. Int. J. Remote Sens. 19, 895–920.
Voogt, J.A., Oke, T.R., 2003. Thermal remote sensing of urban climates. Remote Sens. Environ. 86, 370–384.
Weng, Q., Lu, D., Schubring, J., 2004. Estimation of land surface temperature–vegetation abundance relationship for urban heat island studies. Remote Sens. Environ. 89, 467–483.
White-Newsome, J.L., Brines, S.J., Brown, D.G., Dvonch, J.T., Gronlund, C.J., Zhang, K., Oswald, E.M., O'neill, M.S., 2013. Validating satellite-derived land surface temperature with in situ measurements: a public health perspective. Environ. Health Perspect. 121, 925.
Worcestershire City Council (2015) Warmer Worcestershire Heat Loss Map. (Available:) http://gis.worcestershire.gov.uk/website/warmerworcestershire/ (Accessed 8 August 2015).
Zhou, Y., Shepherd, J., 2010. Atlanta's urban heat island under extreme heat conditions and potential mitigation strategies. Nat. Hazards 52, 639–668.